# Oxygen incorporation in aluminum nitride via extended defects: Part II. Structure of curved inversion domain boundaries and defect formation

Alistair D. Westwooda)

Department of Materials Science and Engineering, Lehigh University, Bethlehem, Pennsylvania 18015

Robert A. Youngman

Carborundum Microelectronics Company, 10409 S. 50th Place, Phoenix, Arizona 85044

Martha R. McCartney

Center for Solid State Science, Arizona State University, Tempe, Arizona 85287

Alastair N. Cormack

New York State College of Ceramics, Alfred University, Alfred, New York 14802

Michael R. Notis

Department of Materials Science and Engineering, Lehigh University, Bethlehem, Pennsylvania 18015

(Received 2 June 1994; accepted 24 January 1995)

Three distinct morphologies of curved (curved, facetted, and corrugated) inversion domain boundaries (IDB's), observed in aluminum nitride, have been investigated using conventional transmission electron microscopy, convergent beam electron diffraction, high-resolution transmission electron microscopy, analytical electron microscopy, and atomistic computer simulations. The interfacial structure and chemistry of the curved and facetted defects have been studied, and based upon the experimental evidence, a single model has been proposed for the curved IDB which is consistent with all three observed morphologies. The interface model comprises a continuous nitrogen sublattice, with the aluminum sublattice being displaced across a  $\{10\overline{1}1\}$  plane, and having a displacement vector  $\mathbf{R} = 0.23(0001)$ . This displacement translates the aluminum sublattice from upwardly pointing to downwardly pointing tetrahedral sites, or vice versa, in the wurtzite structure. The measured value of the displacement vector is between 0.05(0001) and 0.43(0001); the variation is believed to be due to local changes in chemistry. This is supported by atomistic calculations which indicate that the interface is most stable when both aluminum vacancies and oxygen ions are present at the interface, and that the interface energy is independent of displacement vector in the range of  $0.05\langle 0001 \rangle$  to 0.35(0001). The curved IDB's form as a result of nonstoichiometry within the crystal. The choice of curved IDB morphology is believed to be controlled by local changes in chemistry, nonstoichiometry at the interface, and proximity to other planar IDB's (the last reason is explained in Part III). A number of possible formation mechanisms are discussed for both planar and curved IDB's. The Burgers vector for the dislocation present at the intersection of the planar and curved IDB's was determined to be  $b = 1/3(10\overline{10}) + t(0001)$ , where  $t_{\text{meas}} = 0.157$  and  $t_{\text{calc}} = 0.164$ .

#### I. INTRODUCTION

The presence of extended two-dimensional defects with two different morphologies in aluminum nitride (AlN), a planar variant and a curved variant, were first reported by Hagege *et al.*<sup>1</sup> and Westwood and Notis.<sup>2</sup> These two morphologies can exist separately or they can be joined to form complex defects in which the two

crystallographic variants alternate between planar and curved morphologies. In most cases, either when they exist separately or in a more complex morphology, these extended defects are seen to emanate from and terminate at grain boundaries. One subtype of curved defect is a facetted segment that lies on the {1011}. These facetted segments are always observed joined to a basal fault and tend to be quite short. The alternating combination of short facetted segments joined to planar IDB's produces defects which zig-zag through the grain [see Fig. 1(a)]. Another characteristic defect morphology present in AlN

a)Present address: IBM Research Division, T. J. Watson Research Center, Yorktown Heights, New York 10598.

consists of a planar interface joined at both ends by the same curved defect forming a D shape in two dimensions [see Fig. 1(b)]. In three dimensions, this defect encloses a dome-shaped volume of material, and is always contained within a single grain. A dislocation is present at the intersection point of the two defects. Dislocations are sometimes also observed lying in the basal plane of the planar defect.

The extended planar defect lying on the basal plane of the wurtzite AlN structure has received considerable attention from a number of researchers; this interface has been described variously as either an antiphase domain boundary (APB),<sup>3,4</sup> a stacking fault,<sup>1,5,7</sup> or as an inversion domain boundary (IDB),<sup>8–14</sup> which is now known to be the correct structure. For a full description of planar inversion domain boundaries and their possible structures in wurtzite compounds, the authors refer the reader to Part I of this paper.<sup>15</sup>

The curved interface has received very little attention in comparison to the planar defect. The reason for this is likely twofold. The planar fault is an easier interface to analyze using conventional transmission electron microscopy (CTEM), high-resolution transmission electron microscopy (HRTEM), and analytical electron microscopy (AEM), because these techniques require only the interface to be oriented parallel to the beam. Therefore, the crystallographic relationship between the planar defect and the matrix can be more easily obtained. In addition, there is the rationale of first trying to understand the more easily analyzed planar defect structure and chemistry and then applying what was learned in helping to understand the curved interface.

Our understanding of the structure and chemistry of the curved faults is extremely limited. In an identical manner to the planar IDB, they have been described as stacking faults, APB's, and then when Westwood and Notis, susing a convergent beam electron diffraction (CBED) technique<sup>16</sup> allowing the polarity of the crystal to be determined, showed that the polarity of the crystal across the curved interface was reversed through 180°, this unambiguously identified the curved extended defect as an inversion domain boundary (a polarity reversal can only be due to an inversion of the crystal structure). This result was later confirmed independently by Berger<sup>10</sup> and Westwood and Notis<sup>11</sup> using a multibeam technique.<sup>17</sup> Westwood and Notis, 11 using the two-beam invisibility criterion, showed that a displacement vector of R = 1/x(0001) was present. However, these studies provided no information as to the structure of the curved IDB interface.

The existence of different types of curved boundaries was first observed by McKernan and Carter.<sup>3</sup> They indicated that the curved interface was frequently seen to lie on or close to  $\{10\overline{1}1\}$ . Selected area electron diffraction (SAED) patterns obtained from these facetted  $\{10\overline{1}1\}$ 

portions of the curved interfaces showed streaking in the  $\langle 10\overline{1}1\rangle$  across all of the fundamental diffraction spots, including the transmitted spot. The presence of this type of streaking in the diffraction pattern is consistent with diffraction effects arising from plate-like precipitates, in this case lying on  $\{10\overline{1}1\}$ . This result indicated that the facetted portion of the curved interface was likely comprised of a structure and chemistry different from that of the matrix.

Chemical analysis on curved IDB's using analytical electron microscopy (AEM) provided conflicting results. Westwood and Notis<sup>8</sup> showed only a small amount of oxygen to be associated with the curved IDB, Youngman *et al.*<sup>18</sup> provided evidence indicating that a high oxygen concentration was present on the curved IDB. The facetted sections of the curved IDB's have been found to have oxygen concentrations similar to their planar counterparts.<sup>12</sup> These observations suggest that, similar to extended two-dimensional defects in other systems and the planar defect in AlN (a correlation between the presence of the planar defects and oxygen was demonstrated experimentally<sup>8,12,14</sup>), the curved IDB is also related to the presence of impurities.

A planar IDB structure is known to exist in a number of materials, AlN, SiC, 19.20 ZnO, 21-23 GeTe, 24 GaAs, 25 ZnSe, 26 and BeSiN2, 27 However, the curved morphology has been observed only in three materials: oxygencontaining AlN, BeSiN2, 27 and recently in Bi<sub>4</sub>Ti<sub>3</sub>O<sub>12</sub>-doped ZnO. 23 The curved morphology in ZnO was observed in material that had been sintered at 1200 °C. No curved defects were present in material sintered at 900 °C. This observation suggests a processing or temperature dependent formation mechanism. One difference between curved defects in ZnO and AlN is that the defect in ZnO was frequently seen to lie on or close to the prism planes {1010}. In AlN they frequently appear to lie on or close to the pyramidal planes {1011}. However, Youngman<sup>28</sup> has occasionally observed curved IDB segments in AlN lying on the {1010}.

In the system Be<sub>3</sub>N<sub>2</sub>-BeSiN<sub>2</sub>, similar curved defects have been observed, but they were identified as enantiomorphic boundaries.<sup>27</sup> Enantiomorphs are structures that can possess left-handed and right-handed symmetry; an enantiomorphic boundary separates these two different structures. However, enantiomorphic boundaries exist only in lattices where the space group does not contain a "symmetry operation of the second sort," that is, an operation that does not involve an inversion or reflection.<sup>29,30</sup> Wurtzite does possess a mirror plane of symmetry (reflection) and therefore cannot contain enantiomorphic boundaries.

This paper will focus on the study of the curved IDB and its variants in order to elucidate the structure of these interfaces and the relationship to their local chemistry.



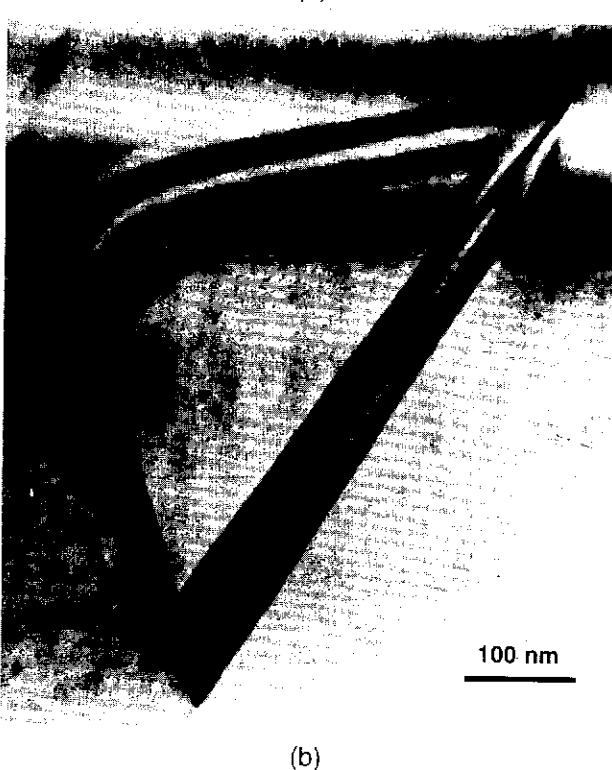


FIG. 1. (a) A DF micrograph showing the alternating zigzag nature of planar and curved IDB's in AIN to form large extended defects (the planar IDB is edge-on to the beam, and the image is along a  $\langle 1\bar{2}10\rangle$  zone axis). (b) A characteristic *D*-shaped defect with the planar IDB being joined at either end by the same curved IDB. A dislocation is present at the points of intersection between the two types of IDB. In three dimensions this *D* will enclose one inverted domain from the other by a flat basal plate with a hemispherical cap.

Results of both experimental studies using a broad range of electron optical and analytical techniques, and theoretical studies using atomistic computer simulations on the curved IDB's, will be presented. Also, this paper will develop a model for the formation of both planar and curved IDB's, starting from the sequence proposed by Harris *et al.*, 9 describing the formation of the octahedral defect complex (the building block of the planar IDB). The description of the defect formation mechanism has been left to this second paper because of the close relationship that is believed to exist between the formation of the planar IDB and the curved IDB; viz., we believe that nucleation of the curved IDB is a direct consequence of the formation of the planar IDB.

#### II. EXPERIMENTAL PROCEDURE

The authors refer the reader to Part I of this paper<sup>15</sup> for a description of the sample preparation, instrumentation, and atomistic computer simulations.

#### III. OBSERVATIONS AND RESULTS

## A. Conventional transmission electron microscopy (CTEM)

The initial studies of Westwood and Notis, <sup>11</sup> using the two-beam invisibility criterion, found four different



FIG. 2. A weak-beam image of a curved IDB using a  $g_{(0002)}$  reflection. The shift in the interface fringe contrast where the extinction contours intersect the fault plane can be clearly seen with the displacement indicated by the arrow.

non-coplanar families of reflections for which curved IDB's lost contrast:  $g_{(1210)}$ ,  $g_{(1100)}$ ,  $g_{(2130)}$ , and  $g_{(3140)}$ . This result was consistent with a displacement along the (0001), in accordance with the zone law, hu + kv +it + lw = 0. CBED patterns taken along the  $\langle 0001 \rangle$ axis from regions of the crystal containing a curved IDB which was oriented normal to the diffraction pattern orientation ((0001)) showed no decrease in symmetry. This result is opposite to that observed in the case of the planar IDB (see Part I, Ref. 15). This confirmed that there was no translation parallel to the basal plane across the curved IDB. However, these observations did not provide any information regarding the magnitude of the displacement along (0001). Further study has been conducted into the magnitude by using a variety of different 000l reflections,  $g_{(0002,4,6,8,10)}$ , which indicated that the magnitude of the displacement was not a rational fraction.

To determine the magnitude of the displacement vector, a weak-beam technique<sup>31,32</sup> was employed, which allows the determination of displacement vectors that need not be described by rational fractions. For an account of the technique, the authors refer the reader to Part I of this paper<sup>15</sup> and the original references above.

A weak-beam image of a curved IDB using a  $g_{(0002)}$  reflection is shown in Fig. 2. Analysis of the curved IDB images revealed a range of magnitudes between  $0.05\langle 0001 \rangle$  and  $0.43\langle 0001 \rangle$  for the displacement vector, which was seen to vary along the same curved IDB. The two-beam technique is suitable only for displacement vectors described by a constant rational fraction of a lattice vector. The variable displacement vector of a

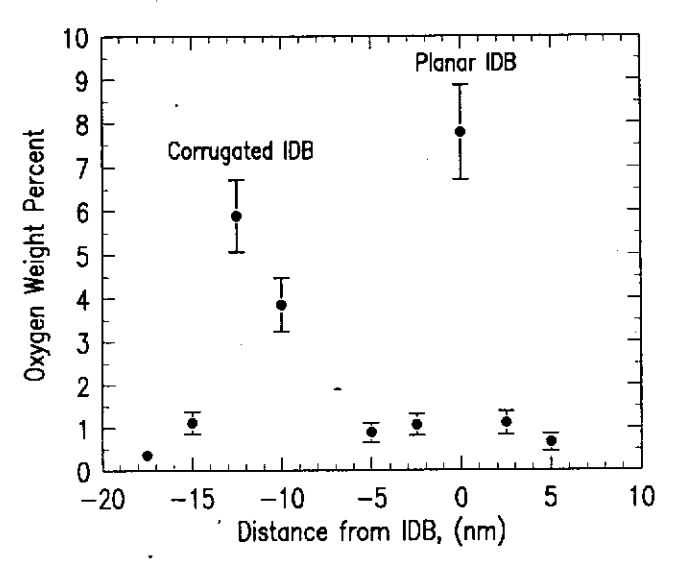


FIG. 3. A quantitative oxygen profile across closely spaced planar and corrugated IDB's. Their respective locations are marked on the profile. An increased oxygen concentration between the pair of IDB's is clearly apparent, producing an asymmetric oxygen profile across the corrugated IDB.

TABLE I. Experimentally determined oxygen concentrations for several curved IDB's.

Curved IDB type	Oxygen weight %	Sample thickness (nm)
Corrugated	5.7 ± 0.8	59
Corrugated	$5.9 \pm 0.9$	. 54
Facetted	$7.3 \pm 1.0$	56
Facetted	$5.7 \pm 0.8$	. 85
Facetted	7.1 ± 1.0	54

nonrational value explains why the two-beam technique was unable to determine the magnitude of the displacement vector.

Confirmation of the experimentally measured displacement vectors using the weak-beam technique requires the matching of experimental images with simulated images of the fringe contrast across the interface.<sup>32</sup> Unfortunately, programs capable of this type of simulation use the Howie–Whelan–Darwin coupled differential equations to calculate the fringe intensity in a crystal due to a given displacement.<sup>33,34</sup> These equations do not allow for changes in crystal potential to be incorporated into the calculations.

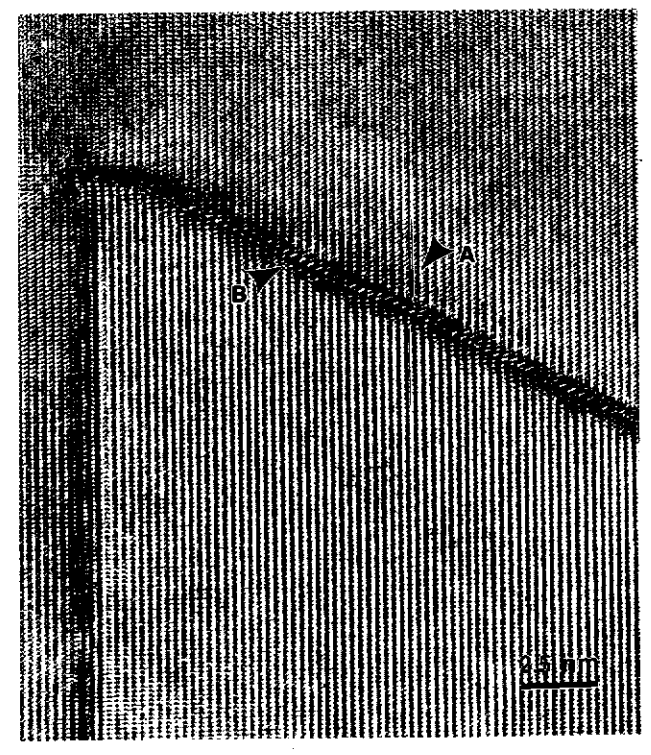


FIG. 4. A high-resolution micrograph ( $\langle 1\overline{2}10 \rangle$  projection) of the intersection between a facetted  $\{10\overline{1}1\}$  curved IDB and a planar IDB (bottom). The image clearly shows a misalignment of the basal planes running across the  $\{10\overline{1}1\}$  facet, corresponding to a *c*-axis displacement (arrow A). A periodic interface structure also appears to be present at the interface (arrow B). Some distortion in the basal planes is present at the intersection in the location of the dislocation. Quantitative image interpretation from this image was impractical because of its large thickness.

Changes in the crystal potential can arise from chemical or structural inhomogeneities, e.g., segregants or precipitates. Calculation of the fringe intensity requires a value for the extinction distance  $(\xi_g)$  for the operating reflection. Because of the changes in crystal potential due to the presence of an oxygen segregant, a reliable value for  $\xi_g$  could not be determined. Therefore, simulations of the fringe contrast could not be carried out and conformation of the experimentally measured displacement vectors could not be obtained.

#### B. Analytical electron microscopy (AEM)

For a full account of the experimental AEM work, the authors refer the reader to Westwood et al. 12.14 Analysis of the curved IDB's revealed oxygen segregation on both the facetted and corrugated morphologies (for a description see Sec. III. C and Part III), with smaller amounts being present on the curved sections. Figure 3 shows a profile across a planar IDB and corrugated fault; the oxygen concentration was found to be 5.7  $\pm$  0.8 wt. % along the corrugated IDB, with quite large variations in concentration being present. Oxygen concentrations along the facetted portion were similar to the planar IDB and can be seen in Table I. The high oxygen concentration observed on the facetted {1011} portions of the curved IDB and the previously reported streaks in diffraction patterns in the directions normal to the {1011} strongly suggest precipitation on these planes. No Monte Carlo electron trajectory simulations, similar

to those described in Part I of this paper<sup>15</sup> were run for the facetted or corrugated IDB's because the input parameters for the program, the structure, width, and density of these boundaries, were not accurately known.

## C. High-resolution transmission electron microscopy (HRTEM)

The facetted IDB structure was chosen for the starting point of the HRTEM study because it fulfilled the necessary imaging criteria; namely that the interface could be tilted parallel to the beam and imaged under a known orientation. Initial observations of the facetted portions of the curved IDB revealed the existence of a periodic structure (see Fig. 4). The images of the facetted portion showed the presence of a c-axis displacement, and no translation in the basal plane. These two observations support the previously obtained CBED and two-beam data.11 A surprising result was that the facetted sections of the curved IDB were found only in the regions of the crystal that were too thick for meaningful interpretation of experimental images by image simulation. The problem of crystal thickness prevented accurate determination of the displacement vector across the facetted IDB. It was observed that as the facetted segment approached thinner regions of the crystal, at the specimen edge, the defect deviated from its {1011} habit plane and exhibited a curved morphology. In these very thin regions of the foil, the curved fault was occasionally found to lie parallel to

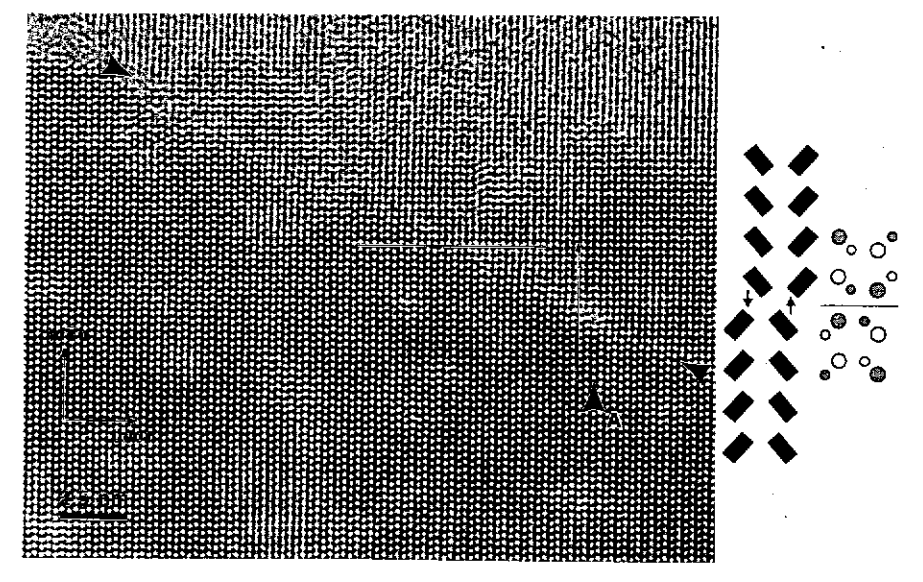


FIG. 5. A high-resolution micrograph of a curved IDB in projection at the edge of the foil ( $(1\overline{2}10)$  projection); the fault lies between the arrows on either side of the micrograph. No basal plane translation is present across the fault as indicated by the central line crossing the IDB. A c-axis translation corresponding to a c-axis displacement of  $0.23\langle0001\rangle$  is present in the arrowed region A. The schematic shows the arrangement of the atomic columns on either side of the interface (black rectangles correspond to the Al-N pair), with the bottom corner of the rectangles in the top domain lining up with the top corner of the rectangles in the bottom domain. This corresponds to the displacement of  $0.23\langle0001\rangle$ . The change in orientation of the rectangles on crossing the IDB is a consequence of the inversion (defocus -49.7 nm; thickness 3.0 nm; atomic columns appear black).

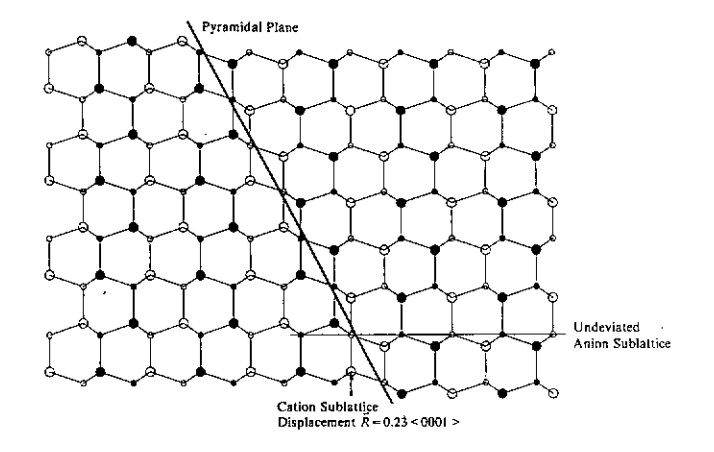
the beam (see Fig. 5). These portions of the crystal allowed quantitative image interpretation of the interface via image simulation. Study of the HRTEM images revealed that the interface had a c-axis displacement of  $\mathbf{R} = 0.23\langle 0001 \rangle$ , no basal plane translation, a nonperiodic structure, and a variable width of 0.2-1.0 nm.

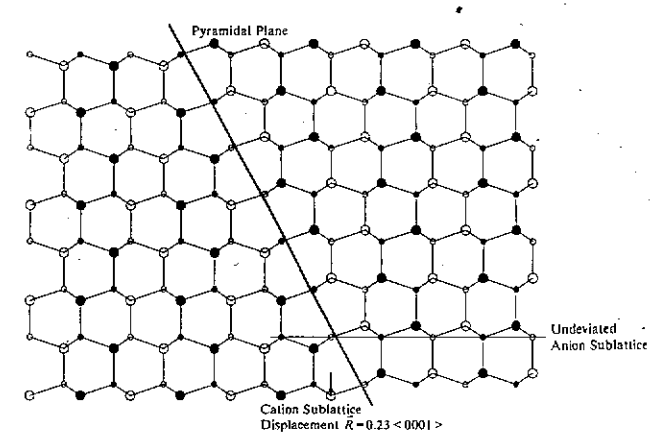
Based upon the experimental observations, a model is proposed to describe the interface structure. Figure 6(a) shows the underlying structure of the interface; a 0.23(0001) displacement of the cation sublattice which translates the aluminum atoms from one type of tetrahedral site to the opposite type of tetrahedral site, fulfilling the inversion requirement; no basal plane translation; and an anion sublattice which is continuous across the interface which is a crystallographic constraint imposed by the fact that the planar IDB is centered upon the cation sublattice. Figures 6(b) and 6(c) are alternate curved IDB interface structures which are both

consistent with the experimental findings: a 0.23(0001) translation of the cation sublattice and an undeviated anion sublattice. The interface in the crystal could be one of these structures, or it could comprise elements form two or all three possible interface configurations.

Figure 7 shows an enlarged region of the interface shown in Fig. 5. Accompanying the micrograph is a schematic trace of the micrograph. The regular matrix is comprised of rectangles which in the image are black solid rectangles produced by the Al-N pairs. Between these two distinct areas, a nonperiodic regions exists which describes the limits of the curved IDB interface. Within this region, two distinctive contrast morphologies are present, a "fuzzy" oval, and solid or diffuse "dumbbell".

Comparison between simulated images (see Fig. 8) of the curved IDB interface structure based upon any of the models shown in Fig. 6, and the experimental





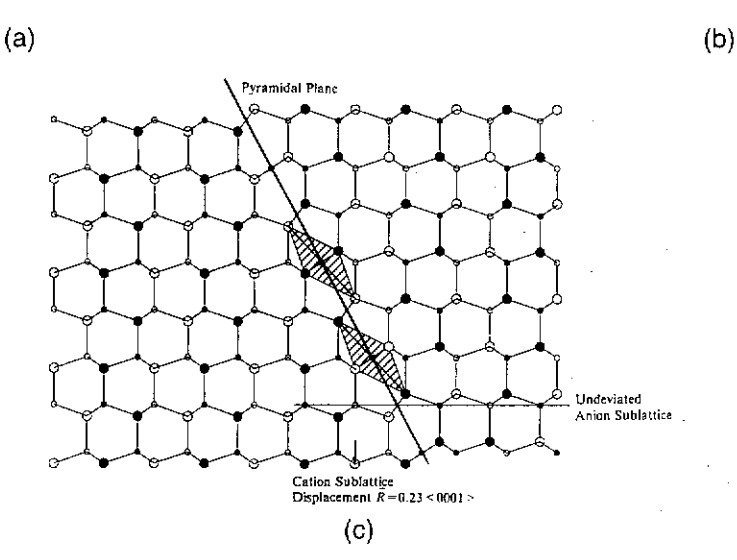


FIG. 6. (a) The underlying structure of the proposed curved IDB interface, based upon HRTEM observation and crystallographic constraints imposed due to the inversion. The nitrogen sublattice is undeviated across the interface, the aluminum sublattice is displaced by 0.23(0001), and no basal plane translation is present, maintaining atomic registry in the c-axis, which is consistent with the conventional microscopy and CBED studies. (b) and (c) are alternate structures of the proposed curved IDB interface. They are consistent with the experimental observations of the interface. In (c) a distorted octahedral structure comprises the repeat unit of the interface similar to that of the planar IDB. [Large circles represent aluminum atoms, small circles nitrogen and/or oxygen (at IDB), and the black atoms are a half plane back.]

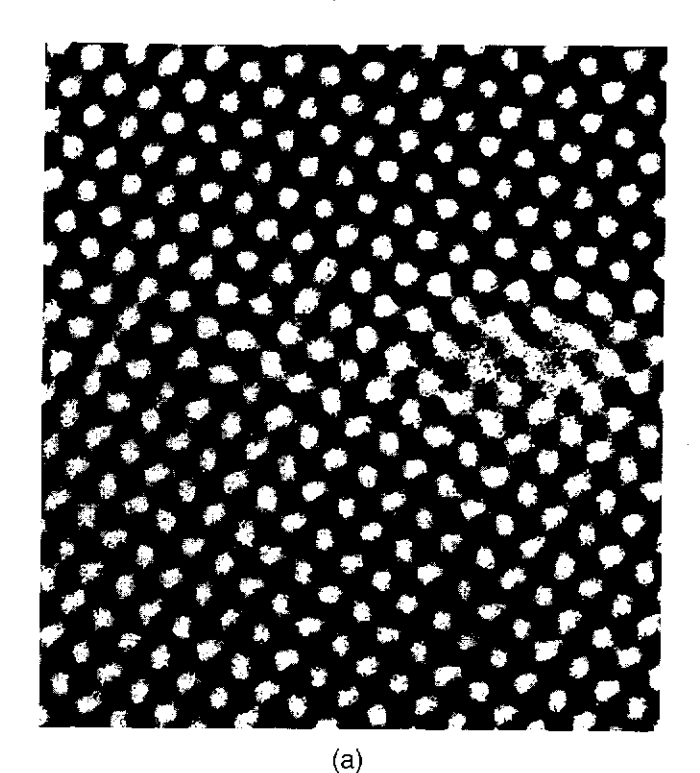


FIG. 7. (a) An enlarged view of the arrowed region A shown in Fig. 5. (b) A trace of the interface clearly highlights the width and structural details contained within the interface. Dark "dumbbells" and diffuse "ovals" are present across the interface instead of the black rectangles produced by the Al-N pairs. These contrast features are commonly observed at the interface.

image in Fig. 7, shows few if any similarities. This apparent discrepancy between the experimental image

and the simulated image based upon the model can be explained, and a much better simulated image can be obtained if we consider the effect of impurities and other defect species. The presence of oxygen on nitrogen sites in the AIN produces a charge imbalance that is compensated by the formation of aluminum vacancies in the ratio of 3 oxygen to 1 vacancy. In the proposed model of Harris et al.,9 the formation of octahedral aluminum-oxygen complexes would further reduce the oxygen to aluminum vacancy ratio to 9 oxygen to 1 vacancy. This would still leave a high concentration of aluminum vacancies. AEM confirmed previous observations of oxygen associated with the various curved IDB morphologies. Also, the structural model of the curved IDB contains closely spaced cation sites 0.224 nm (equilibrium spacing in AlN is 0.311 nm) across the interface. These would be highly unstable sites, and it is suspected that aluminum vacancies would occupy one of the two sites. This was later supported by the atomistic computer simulation data.

A consequence of this reasoning was to study the effects of chemistry on the simulated images, in particular, the effect of aluminum vacancies. The presence of oxygen at the interface was ignored because it would have little effect on the image contrast because of the similar size, mass, and scattering power to that of nitrogen. It was found that an aluminum vacancy produced a fuzzy oval contrast, and closely spaced aluminum atoms on either side of the interface produced dumbbell type contrast features, as shown in Fig. 9. These match very well with those contrast features in Fig. 7. The simulated image in Fig. 9 is 3.0 nm thick with each column of atoms containing 10 atoms. The columns in the simulated image exhibiting the fuzzy oval. structure contain five vacancies and five atoms: therefore. the site occupancy of these columns is 0.5.

In comparing the simulated and experimental images, it appears that the proposed model provides the

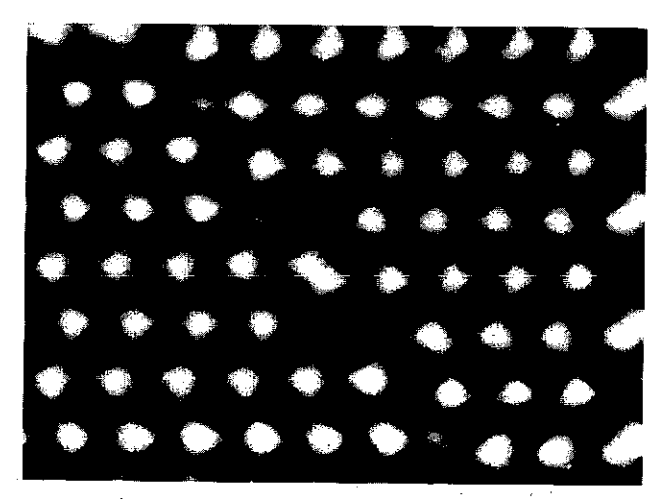
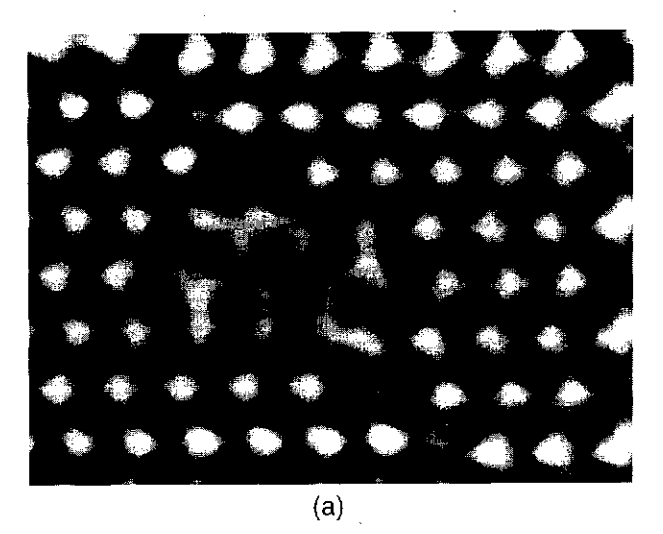


FIG. 8. A simulated image of the interface structure in Fig. 6(a).

basic structural framework onto which the chemistry, i.e., the aluminum vacancies, must be superimposed. Also, crystallographic considerations must be added in the form of jogs and kinks along the {1010}, {1011}, and {0001} and other planes because on the atomic scale, a curved interface must ultimately be facetted. An exact simulation of experimental images is virtually impossible, owing to the very large number of possible interface structures. If we consider a 3.0 nm thick foil, each projected atomic column would contain =10 atomic sites of which all, some, or none could be occupied by an aluminum vacancy, and then this must be applied to each atomic column in the experimental image with the result of there being =100,000 possible interface structures.



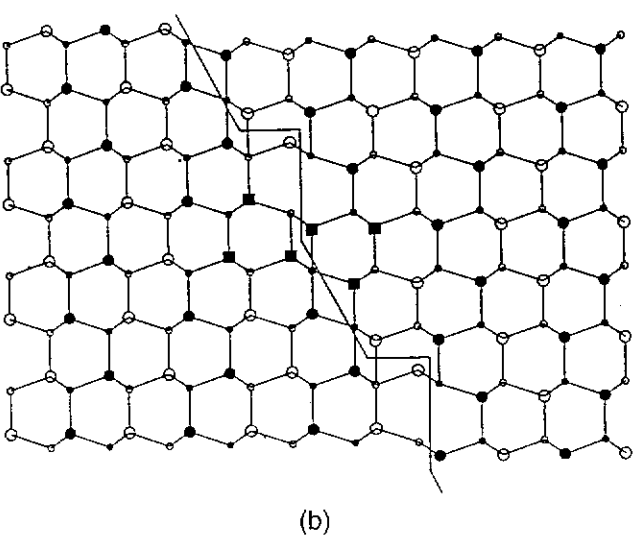


FIG. 9. (a) The simulated image of the accompanying interface structure (b) shows the effects of introducing aluminum vacancies (black squares) to the interface, producing diffuse ovals. The experimentally observed "dumbbells" can be created when AI-N pairs are in close proximity to each other. Facetting on an atomic scale can be seen, which will ultimately produce a curved IDB at the macroscopic scale. [Large circles represent aluminum atoms, small circles nitrogen and/or oxygen (at IDB), and the black atoms are a half plane back.]

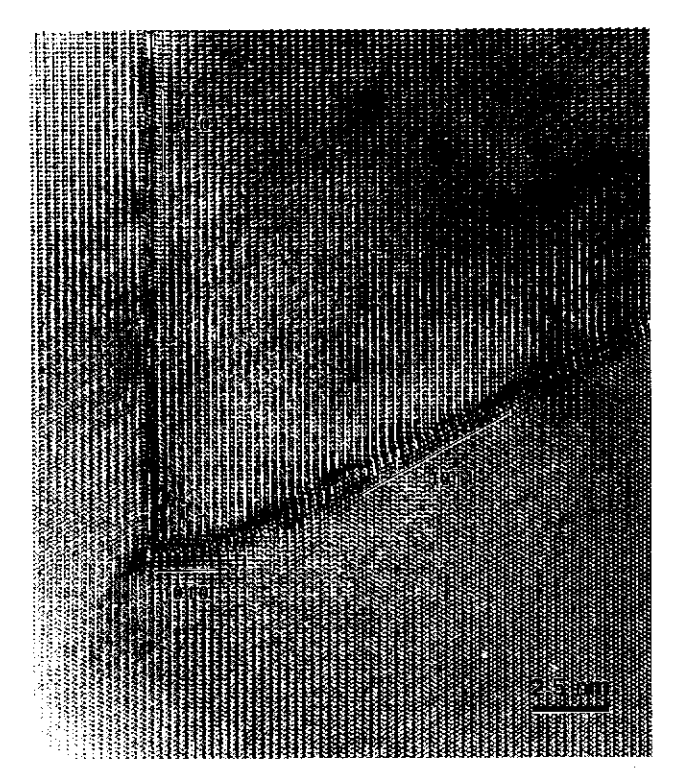


FIG. 10. A short {1010} prism facet was observed at all the intersections between curved/facetted IDB's and planar IDB's. The Burgers vector for the dislocation at the intersection is determined by the sum of the respective displacement vectors. Because the curved IDB is of variable magnitude, the Burgers vector of the dislocation would also vary. Therefore, the presence of the ~2.5 nm long facet would allow the Burgers vector for the dislocation to be fixed because the translation across the prism facet would be of a fixed displacement.

A further complication to the matching of simulated with experimental images is atomic relaxations at the interface; these are most certainly present here due to the presence of vacant sites, altered coordination, and changes in chemical species at the interface.

Three further observations regarding the curved IDB are, first, a very short ( $\simeq 2.5$  nm)  $\{10\overline{1}0\}$  facet was seen at the intersection point between the planar and facetted  $\{10\overline{1}1\}$  IDB's, as shown in Fig. 10. Second, a third variant of the curved IDB was observed which was broad and appeared to have a corrugated or undulating nonperiodic structure. This corrugated variant was seen to lie parallel to the planar IDB, as shown in Fig. 11. Third, the relative stability of the curved IDB is less than the planar IDB, this observation being based on the disappearance of the curved IDB at the foil edge, while the planar IDB maintained its structure up to the foil edge, and that the facetted IDB always deviated from the  $\{10\overline{1}1\}$  on approaching the specimen edge.

#### D. Atomistic computer simulations

The purpose of the atomistic computer simulations was to probe further the curved IDB structure and

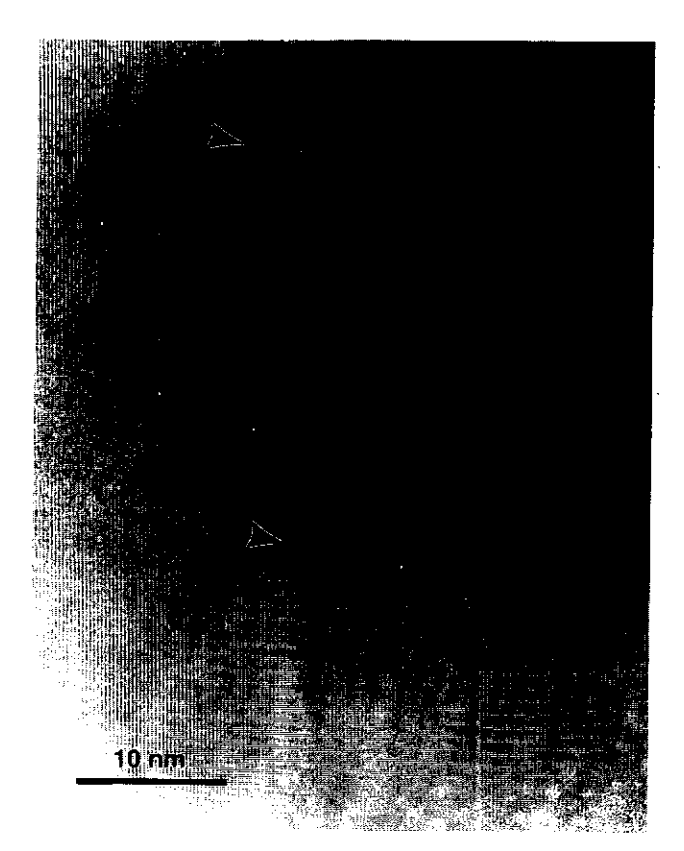
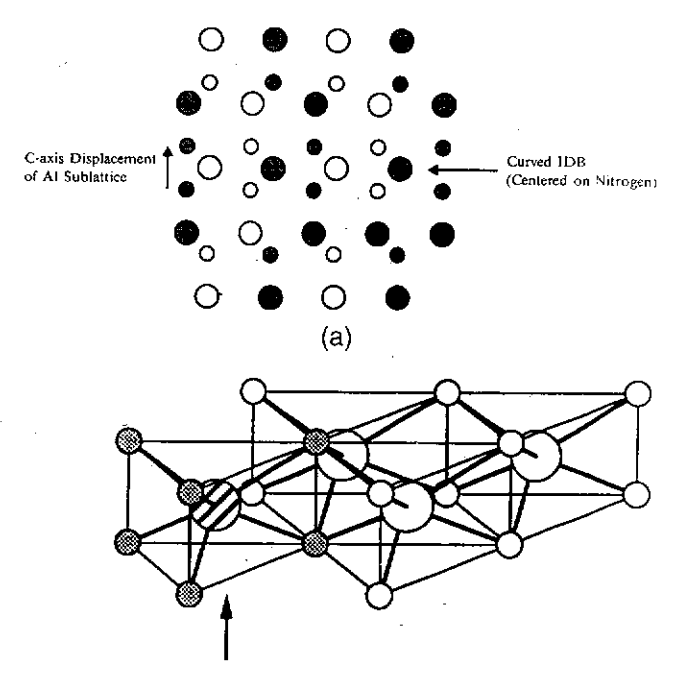


FIG. 11. A high-resolution micrograph showing a corrugated IDB (arrowed) adjacent to a planar IDB. Curved IDB's were occasionally observed to lie parallel to a planar IDB, and when this occurred the curved IDB would tend to show a corrugated or rippled structure.

chemistry. The leading problem that was faced was the choice of the initial structure for the curved IDB. Based upon the experimental observations, the crystallographic constraints imposed by the wurtzite structure, and the presence of the planar IDB centered upon the aluminum sublattice, the curved IDB structure that was used as the input for the supercell is shown in Fig. 12. The structure consisted of a prismatic arrangement of aluminum atoms surrounding a sixfold coordinated nitrogen atom, with the cation sublattice displaced by  $\mathbf{R} = 0.23\langle 0001 \rangle$ . These calculations were conducted using a supercell in which the curved IDB structure was lying on the basal plane. This supercell construction was realistic of some, but not all curved IDB structures, because the curved IDB must at some locations lie on portions of the basal plane. Also, the corrugated IDB was observed to lie close to the basal plane, lending additional support for the choice of supercell geometry.

The influence of aluminum vacancies on the energy of the curved IDB was studied first, followed by the effect of oxygen. The curved IDB interface was most energetically stable when the aluminum vacancies were present in those planes adjacent to the IDB interface plane. The other interface parameter adjusted was the displacement vector of the aluminum sublattice. Origi-



Structural Unit of the Curved IDB Six-fold Coordinated Nitrogen (b)

FIG. 12. (a) A  $\langle 1\overline{2}10 \rangle$  projection of the initial input structure of the curved IDB. (b) shows that the structure in (a) is based upon a highly energetic sixfold coordinated nitrogen in a prismatic arrangement. [Small circles represent aluminum atoms, large circles nitrogen and/or oxygen (at IDB), and the shaded atoms are a half plane back.]

nally at  $\mathbf{R}=0.23\langle0001\rangle$ , it was varied from  $0.05\langle0001\rangle$  to  $0.61\langle0001\rangle$ . Figure 13 shows the plot of energy versus displacement. An energy minimum was observed for the curved IDB when a displacement of  $\mathbf{R}\simeq0.23\langle0001\rangle$  was present.

Initially, oxygen was substituted for nitrogen at the center of the curved IDB structure. This was found to decrease the stability of the interface. The oxygen was then located in the adjacent nitrogen-containing basal planes, with the result that this configuration was found to be the most stable (see Fig. 14). The effect of oxygen on the displacement vector at the interface was studied, as was previously described in the case of just aluminum vacancies. Figure 13 shows the combined effect of aluminum vacancies and oxygen. Oxygen can be seen to have a dramatic effect on the stability of the curved IDB. No energy minima were found at specific interface displacements; instead, an energy plateau of constant energy was observed for a range of displacement vectors. The stability of the curved IDB was seen to be constant for  $\mathbf{R} = 0.10\langle 0001 \rangle$  to  $\mathbf{R} = 0.35\langle 0001 \rangle$ . The energy plateau can be seen to be much greater than the energy minima associated with just aluminum vacancies present at the interface, again indicating the large effect that oxygen has on stabilizing the curved IDB. The output

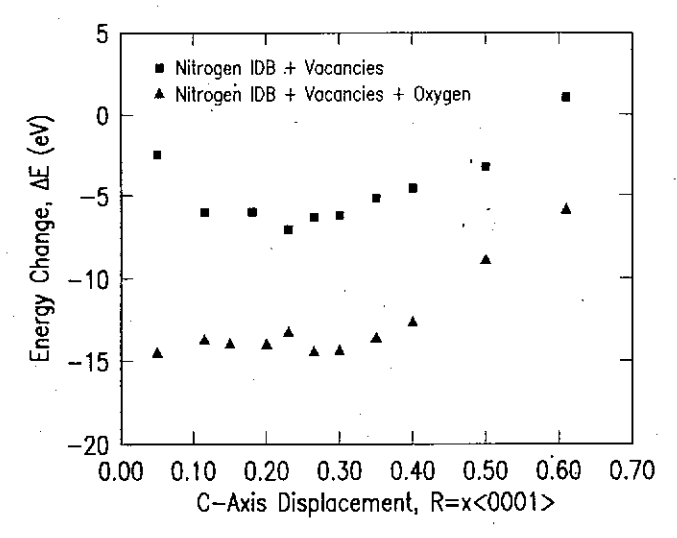


FIG. 13. A plot of change in energy as a function of c-axis displacement for the curved IDB under differing imposed chemistries. The energy change is the difference between the initial energy of the input structure and the minimized energy of the output structure for the interface. The influence of vacancies can be seen in the top curve with a minimum in energy being observed when the displacement is 0.23(0001). This supports the observed experimental results. The bottom curve shows the influence of the oxygen solute cloud. The presence of the oxygen creates an interface with an energy independent of the displacement between  $0.05\langle 0001 \rangle$  and  $0.35\langle 0001 \rangle$ . This result is also in agreement with fringe displacements measured via weak beam, showing a variable displacement.

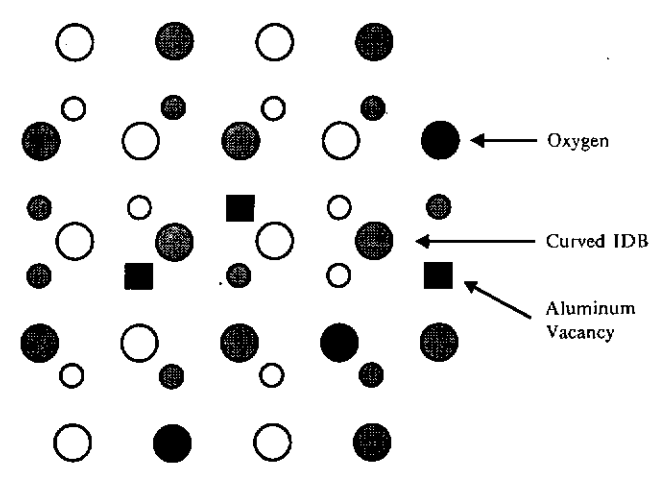


FIG. 14. A schematic of the structural arrangement of the cured IDB input as the starting structure. The aluminum vacancies ( ) were input at the interface, and the oxygen was found to prefer sites adjacent to the interface. The interface was found to be less stable when oxygen was located at the center of the IDB. (Small circles represent aluminum atoms, large circles nitrogen, the shaded atoms are a half plane back, and the large black circles are oxygen.)

structure of the curved IDB showed a disordered region of nitrogen and aluminum, which was possibly trying to maintain some degree of tetrahedral bonding, the amount being limited by the necessary inversion and the high concentration of aluminum vacancies. These atomistic calculations are consistent with the weak-beam observations of a variable displacement vector and the AEM data, indicating the presence of oxygen at the curved IDB's. It also supports our decision to investigate the effect of aluminum vacancies on the HRTEM image simulations of the curved interface.

#### E. Dislocation analysis

Dislocations are present at the intersection between all curved IDB's and planar IDB's. Information on the type of dislocation and its Burgers vector (b) can provide insight into the defect displacement and possible defect formation mechanisms; for example, Frank dislocations are produced by either coalescence and collapse of vacancies or segregation of interstitials.

Simple dislocation analysis using three different noncoplanar reflections for which the dislocation lost contrast was not possible because for all reflections except  $g_{(1210)}$  fringe contrast was always present, which masked the dislocation contrast. Cheng et al., 35 examining dislocations at intersecting planar IDB's in SiC, determined that the Burgers vector of a dislocation was related to the displacement vectors of the two intersecting IDB's by  $b = \mathbf{R}_1 - \mathbf{R}_2$ . This corresponds to  $b = \mathbf{R}_{planar} - \mathbf{R}_{curved}$  in this system. In considering what R to use for the curved IDB, it is important to remember the small  $\{10\overline{10}\}$  facet that was observed at the intersection of the planar and curved IDB's (see Fig. 10). It is believed that this facet fixed the magnitude of the displacement vector of the curved IDB at  $\mathbf{R} = 0.23(0001)$  at the intersection point, irrespective of the curved IDB displacement vector at various locations along its length. Therefore, the Burgers vector of the dislocation at the intersection of the planar and curved IDB's can be determined,  $b = 1/3(10\overline{10}) +$ t(0001). Taking the experimentally measured and calculated values for the c-axis component of the planar IDB displacement vector,  $t_{\text{meas}} = 0.157$ , with  $t_{\text{calc}} = 0.164$ . A dislocation with either of these Burgers vectors is expected to be sessile, anchoring the planar and curved IDB's to the dislocation's location in the lattice. Only through climb could it be removed from the lattice, and in doing so may generate the {1010} IDB's observed by Youngman.<sup>28</sup>

#### IV. NUCLEATION AND GROWTH MECHANISMS

In this section a theory will be developed describing the nucleation and growth of the planar and curved IDB's. There are a number of possible nucleation mechanisms that can be categorized as coalescence and precipitation, sintering-related, and powder synthesis related. The theory to be presented here will focus on the coalescence and precipitation mechanism.

On cooling from the AlN processing temperature, the matrix becomes an oxygen-containing supersaturated solid solution, containing the octahedral defect clusters. As the temperature decreases, it becomes more favorable for coalescence and precipitation of these clusters to occur, rather than for them to sit randomly in the AIN matrix. The clusters prefer to precipitate out on the basal plane because this produces the least amount of distortion and strain within the lattice. The precipitation produces an oxygen-rich platelet, which creates a stacking fault as shown in Fig. 15(a). No inversion is present at this early stage.

A simple but effective method of analyzing is to use Pauling's rule of electrovalency. <sup>36</sup> In the regular AlN structure, the bond strength (charge on nucleus/number of bonds) for Al is +3/4; this is balanced by N with -3/4. There is a net negative charge of -6/16 per Al atom at the planar IDB. However, those Al atoms sitting in the basal plane marked  $A_1$  possess a net positive charge of +3/16. The Al atoms in the basal plane marked  $A_2$  possess a net positive charge of +8/16, which can be seen to provide a overall positive charge of +5/16

for the IDB. This structural configuration is not stable, in particular because of the large positive charge on the  $A_2$  basal plane atoms. This unstable configuration can be made more stable and electrically neutral by those Al atoms in  $A_2$  switching tetrahedral sites from upwardly pointing to downwardly pointing, as indicated in Fig. 15(b). In these new sites, the aluminum atoms possess a reduced net positive charge of +3/16. The planar interface is now electrically neutral, with the -6/16 charge being balanced by +3/16 on either side of the interface. The switching of Al tetrahedral sites creates an inversion across the planar IDB and in doing so creates the curved IDB [see Fig. 15(c)]. Therefore, the nucleation of the curved IDB interface is a direct consequence of the stabilization mechanism of the planar interface, which in itself is a direct metamorphosis of a stacking fault to an inversion domain boundary.

The switching of the aluminum sites can also be accomplished by a translation of  $1/3\langle 10\overline{10}\rangle + 0.27\langle 0001\rangle$ . This switching of aluminum sites will occur only when

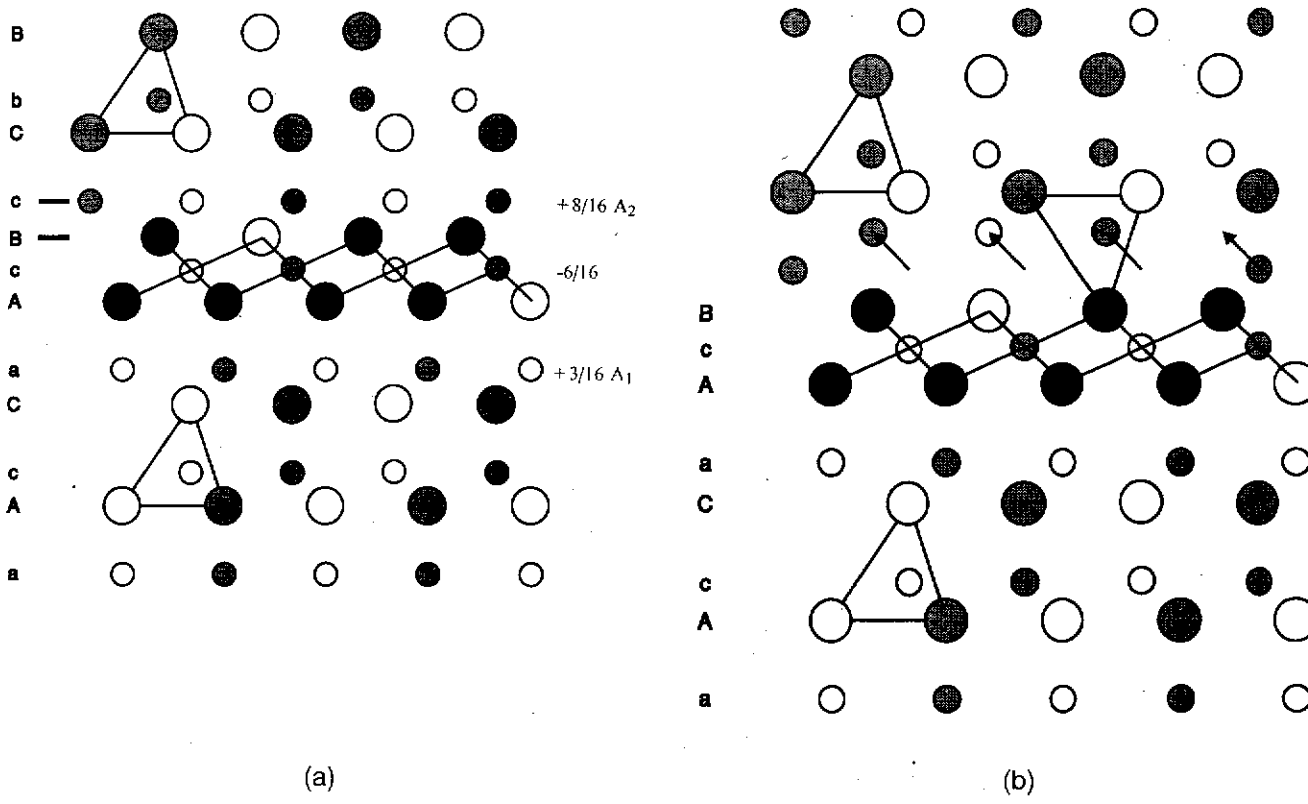


FIG. 15. A formation mechanism for the planar and curved IDB's is outlined based upon precipitation of the octahedral clusters on the basal plane of the AlN structure. (a) Precipitation of octahedral clusters on the basal plane. This creates two adjacent stacking faults, leaving a plane of aluminum atoms in unfavorable sites. The fractions on the right-hand side refer to the average charge on an aluminum ion in the plane. It is obvious that the defect is not electrically neutral and the aluminum atoms in plane  $A_2$  are in unfavorable sites. (b) A simple translation of those aluminum atoms in  $A_2$  from one tetrahedral site to the opposite tetrahedral site creates an inversion across the planar IDB and also produces an electrically neutral interface. (c) A direct consequence of the translation in (b) is the creation of the curved IDB because the inversion domain formed by the translation of the aluminum atoms produces a second IDB (curved) at the point where aluminum atoms which have been translated meet with the aluminum sublattice which has not been translated. Note: for simplicity, the short  $\{10\overline{10}\}$  facet observed experimentally at the intersection between the planar and curved IDB's has been omitted. (Small circles represent aluminum atoms, large circles nitrogen, the shaded atoms are a half plane back, and the large black circles are oxygen.)

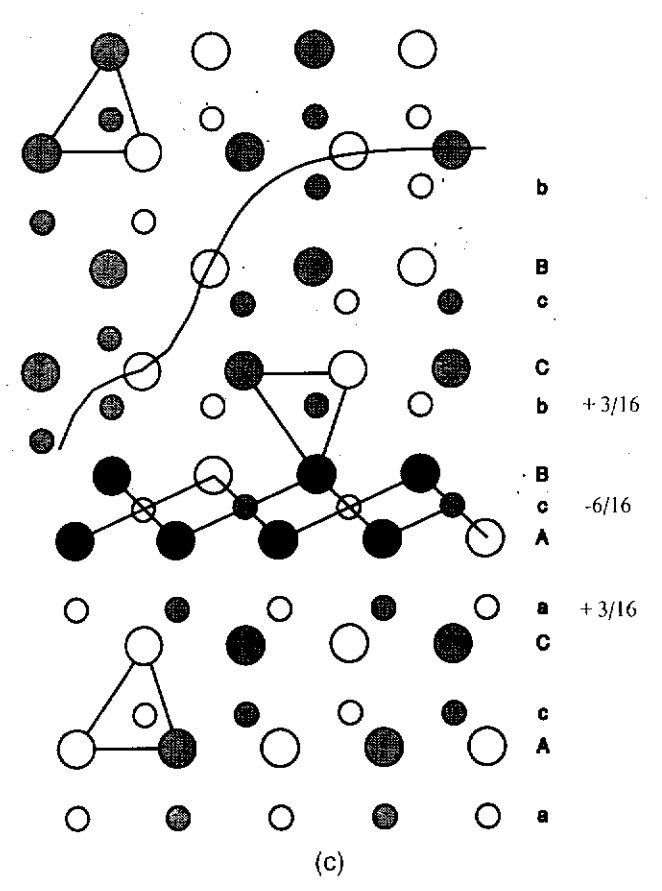


FIG. 15. (continued from previous page)

there is an overall increase in the stability of the system, which occurs when the increase in stability of the planar interface caused by the aluminum atoms sitting in their new sites is greater than the energy of the newly formed curved IDB interface. A critical stacking fault platelet size is likely required. Above this size a curved IDB could spontaneously nucleate and grow. Below this critical size a curved IDB could not nucleate and grow, unless through continued precipitation of octahedral defects the stacking fault platelet reached the critical size.

The mechanisms and driving forces for growth of the planar and curved IDB's have been described in the preceding paragraphs. The underlying assumption for the driving force for the formation of the planar fault is the overall reduction in the internal energy between the two states; the high energy state being the supersaturated oxygen-rich matrix, and the lower energy state which has removed the supersaturated oxygen-rich matrix by precipitation of the oxygen-rich octahedral complexes, forming the planar fault with a lower oxygen concentration still present in the matrix. It is suggested that the driving forces for the formation of the curved IDB are based on the balancing of an initial charge imbalance at the planar fault. These two formation

schemes for the planar and curved IDB's are consistent with the experimental data.

In considering the growth mechanisms of these two types of IDB, the planar is the easier case to consider. Two possible mechanisms can be suggested. First, the fault continues to expand by growing into supersaturated oxygen-rich regions from which additional oxygen complexes can precipitate out onto the basal plane of the fault. The second mechanism is that the fault acts as a high diffusion path, allowing oxygen from a source, e.g., grain boundaries, to diffuse rapidly down the fault to the edge, where it continues to grow into the matrix. These two mechanisms are known to occur in various systems. A far more difficult problem is faced in trying to explain the growth of the curved IDB both parallel and normal to the planar fault. It is less clear in the case of the curved IDB the influence of chemistry on the final morphology, and the role that other adjacent planar IDB's may have on their growth characteristics. Another question is how the relationships that may exist between the growth mechanisms for the planar and curved IDB's affect the final morphologies. A great deal of research into the nucleation and growth of these defects is still required. The main problem facing research in this area is the inhomogeneous oxygen distribution present in the samples. Control of the oxygen distribution is the key

### Oxygen-rich Precipitate Comprised of Octahedral Defects

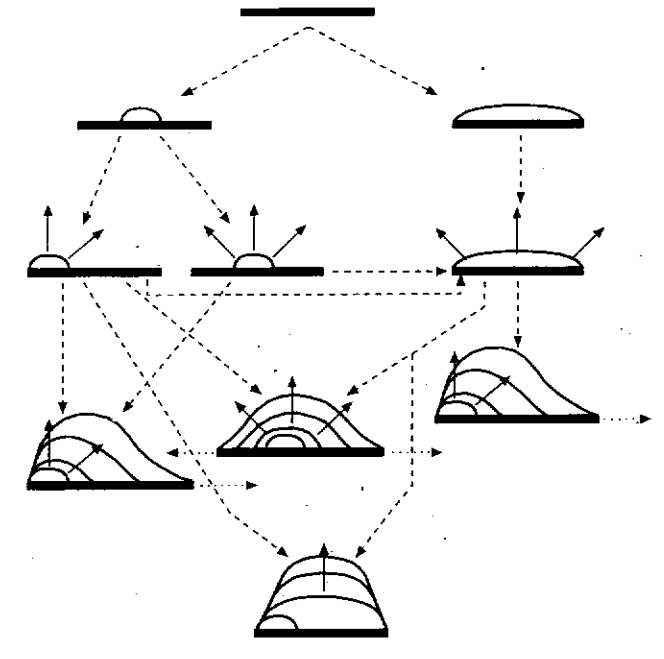


FIG. 16. A schematic describing some of the possible nucleation and growth processes that can be envisaged for the curved and planar IDB's. Solid and dotted arrows indicate the growth direction of the curved and planar IDB's, respectively. The dashed arrows indicate the next step in the suggested growth process.

to successful experiments in this area. Figure 16 shows some of the possible permutations for the growth of the curved and planar IDB's.

#### V. CONCLUSIONS

Three morphologically distinct variants—curved, {1011} facetted, and corrugated—comprise the complex structure of the curved IDB interface. The curved IDB possesses a displacement vector of variable magnitude, and the facetted segments exhibited a displacement vector of 0.23(0001), but the displacement vector for the corrugated variant is unknown. A model has been proposed that provides a basic frame work for understanding the relationship of these structures to the chemistry of the system. This model is composed of a continuous anion sublattice across the interface, the cation sublattice being displaced by  $\mathbf{R} = 0.23\langle 0001 \rangle$ , which translates the aluminum sublattice from one type of tetrahedral site to the other type of tetrahedral site, and the interface plane being composed of nitrogen atoms on the  $\{10\overline{11}\}$ . Superimposed upon this basic structure are the fluctuations in chemical composition (oxygen and aluminum vacancies) around the interface. The local changes in chemistry are believed to control the curved IDB's final morphology.

The atomistic computer simulations support this argument, with the results showing that aluminum vacancies adjacent to the interface and oxygen in the form of a solute "cloud" stabilize the interface. Additional calculations showed that the interface did not prefer a fixed displacement vector, and that a stable interface was found to exist over a wide range of displacements,  $\mathbf{R} = 0.05\langle0001\rangle$  to  $\mathbf{R} = 0.35\langle0001\rangle$ , which certainly explains the variable displacement vector that was measured. Also, this variability in interface displacement allows for a greater flexibility in interface structure, thus enabling the curved IDB to assume a number of different morphologies.

The dislocation at the intersection between the planar and curved IDB's has a Burgers vector of  $b = 1/3\langle 10\overline{10}\rangle + t\langle 0001\rangle$ , where  $t_{\text{meas}} = 0.157$  and  $t_{\text{calc}} = 0.164$ . The dislocation maintains a fixed displacement due to the presence of a small  $\{10\overline{1}1\}$  facet at the intersection point. The deviation of the facetted fault from its habit plane in thin areas was a surprising result. The reason for this is not apparent, but the relaxation of strain associated with the interface is the likely cause.

#### **ACKNOWLEDGMENTS**

The authors wish to thank the Semiconductor Research Corporation (SRC) and British Petroleum America for funding this work, Dr. J.R. Michael for assistance with the Monte Carlo simulations,

Dr. S. Witek for supplying the undoped hot-pressed AlN sample, and the external users program at the Center for High-Resolution Electron Microscopy at Arizona State University.

#### REFERENCES

- S. Hagege, Y. Ishida, and S. Tanaka, ISE Grain Boundary Meeting, July 1987, Lake Placid, NY (1987).
- A. D. Westwood and M. R. Notis, Adv. Ceram. 26, 171-187 (1989).
- S. McKernan and C. B. Carter, in Advanced Electronic Packaging Materials, edited by A. T. Barfknecht, J. P. Partridge, C. J. Chen, and C-Y. Li (Mater. Res. Soc. Symp. Proc. 167, Pittsburgh. PA. 1989), pp. 289-294.
- S. McKernan, M. G. Norton, and C. B. Carter, in *High Resolution Electron Microscopy Defects in Materials*, edited by R. Sinclair, D. J. Smith, and U. Dahmen (Mater. Res. Soc. Symp. Proc. 183. Pittsburgh, PA, 1990), pp. 267-272.
- S. Hagege, S. Tanaka, and Y. Ishida, J. Phys. 49, C5, 189-194 (1988).
- S. Hagege, S. Tanaka, and Y. Ishida, J. Jpn. Inst. Metals 52, 1192-1198 (1988).
- 7. S. Hagege and Y. Ishida, Philos. Mag. A 63, 241-258 (1991).
- A. D. Westwood and M. R. Notis, in Advanced Electronic Packaging Materials, edited by A. T. Barfknecht, J. P. Partridge, C. J. Chen, and C-Y. Li (Mater. Res. Soc. Symp. Proc. 167, Pittsburgh. PA, 1989), pp. 295–300.
- J. H. Harris, R. A. Youngman, and R. G. Teller, J. Mater. Res. 5. 1763–1773 (1990).
- 10. A. Berger, J. Am. Ceram. Soc. 74, 1148-1151 (1991).
- A. D. Westwood and M. R. Notis, J. Am. Ceram. Soc. 74, 1226–1239 (1991).
- A. D. Westwood, J. R. Michael, and M. R. Notis, in *Microbeam Analysis 1991*, edited by D. G. Howitt (San Francisco Press, San Francisco, CA, 1991), pp. 245-249.
- M. R. McCartney, R. A. Youngman, and R. G. Teller, Ultramicrosc. 40, 291-299 (1992).
- A. D. Westwood, J. R. Michael, and M. R. Notis, J. Microsc. 167, 287–302 (1992).
- A. D. Westwood, R. A. Youngman, M. R. McCartney, A. N. Cormack, and M. R. Notis, J. Mater. Res. 10, 1270–1286 (1995).
- J. Tafto and J. C. H. Spence, J. Appl. Crystallogr. 15, 60-64 (1982)
- M. Snykers, R. Serneels, P. Delavignette, G. Gevers, J. Van Landuyt, and S. Amelinckx, Phys. Status Solidi A 41, 51-63 (1977).
- R. A. Youngman, J. H. Harris, P. A. Labun, R. J. Graham, and J. K. Weiss, in *Advanced Electronic Packaging Materials*, edited by A. T. Barfknecht, J. P. Partridge, C. J. Chen, and C-Y. Li (Mater. Res. Soc. Symp. Proc. 167, Pittsburgh, PA, 1989), pp. 301–306.
- P. Pirouz, C. M. Chorey, and J. A. Powell, J. Appl. Phys. Lett. 50, 221–223 (1987).
- W. R. L. Lambrecht and B. Segall, Phys. Rev. B 41, 2948–2958 (1990).
- 21. J. C. Kim and E. Goo, J. Am. Ceram. Soc. 73, 877-884 (1990).
- J. Bruley, U. Bremer, and V. Krasevec, J. Am. Ceram. Soc. 75, 3127–3128 (1992).
- K. Makovec and M. Trontelj, J. Am. Ceram. Soc. 77, 1202-1208 (1994).
- M. Snykers, P. Delavignette, and S. Amelinckx, Mater. Res. Bull. 7, 831–840 (1972).
- Z. Liliental-Weber, M. A. O'Keefe, and I. Washburn, Ultramicrosc. 30, 26-30 (1989).

- M. Shiojiri, C. Kaito, S. Sekimoto, and N. Nakamura, Philos. Mag. A 46, 495-505 (1982).
- 27. T. M. Shaw and G. Thomas, J. Solid State Chem. 33, 63-82 (1980)
- 28. R. A. Youngman, private communication (1991).
- P. Goodman and T. W. Secomb, Acta Crystallogr. A 33, 126–133 (1977).
- O. Van der Biest and G. Thomas, Acta Crystallogr. A 31, 70-76 (1975).
- 31. K. Miyazawa and Y. Ishida, Ultramicrosc. 22, 231-238 (1987).
- K. Miyazawa, Y. Ishida, and T. Suga, Philos. Mag. A 58, 825-832 (1988).
- D. R. Rasmussen and C. B. Carter, J. Electron Microsc. Tech. 18, 429–436 (1989).
- 34. D. R. Rasmussen, N. Cho, D. W. Susnitzky, and C.B. Carter, Ultramicrosc. 30, 27–32 (1989).
- T. T. Chen, P. Pirouz, and F. Ernst, in Advances in Materials, Processing and Devices in III-V Compound Semiconductors, edited by D. K. Sadana, L. Eastman, and R. Dupuis (Mater. Res. Soc. Symp. Proc. 144, Pittsburgh, PA, 1989), pp. 189-194.
- L. Pauling, The Nature of the Chemical Bond (Cornell University Press, Ithaca, NY, 1960), pp. 64–107.